Microelectronic Engineering 283 (2024) 112116

Contents lists available at ScienceDirect

Microelectronic Engineering

journal homepage: www.elsevier.com/locate/mee

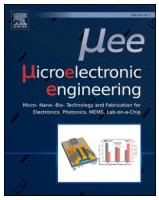

Advanced approach of bulk (111) 3C-SiC epitaxial growth

C. Calabretta [a,b,*], V. Scuderi [a], C. Bongiorno [a], R. Anzalone [b], R. Reitano [c], A. Cannizzaro [a,b], M. Mauceri [d], D. Crippa [e], S. Boninelli [a], F. La Via [a]

[a] CNR-IMM, VIII Strada, 5, 95121 Catania, Italy
[b] STMicroelectronics, Stradale Primosole 50, 95121 Catania, Italy
[c] DFA, Università degli studi di Catania, Via S. Sofia 64, 95123 Catania, Italy
[d] LPE, Strada XVI, Catania, Italy
[e] LPE, via Falzarego 8 Baranzate (MI), Italy

ARTICLE INFO

Keywords:
(111) 3C-SiC
CVD growth
TEM
Photoluminescence
Stacking faults

ABSTRACT

3C-SiC films grown on (111) Si substrates exhibit poor crystal quality and experience wafer cracks and bowing preventing access to bulk growth. This work reports innovative Chemical Vapor Deposition (CVD) growth methodology on 4 in. Si substrates which allowed the growth of 230 mm thick layer of (111) 3C-SiC through the melting of the Si substrate in the CVD chamber and the adoption of the resulting free standing 3C-SiC for the growth of bulk (111) 3C-SiC layer under high N fluxes. From the molten KOH etching and subsequent SEM investigation it has been ascertained that with a N_2 flux of 1600 sccm there is a significant reduction in the concentration of stacking faults (SFs) from $(7.16 \pm 0.04) \times 10^3$ cm^{-1} to $(0.4 \pm 0.3) \times 10^3$ cm^{-1}. This reduction is consistent with the cross section m-PL response displaying steep and uniform increase in the intensity of the band-edge signal a factor 10 higher on the surface with respect to the equal (100) 3C-SiC grown thickness. Furthermore, the emission attributed to point defects is considerably lower in (111) 3C-SiC. From Scanning Transmission Electron Microscopy (STEM) investigation it appears evident how the typical mechanism valid in (100) growths consisting in the mutual closure of SFs coming from opposing {111} planes that give rise to Lomer and l-shaped dislocations is replaced by a different panorama of evolution. Indeed, it is shown how the SFs shred but do not interrupt each other during growth. Furthermore, dropping in the number of atomic planes composing SFs layers appears to be a key phenomenon leading to both the shrinkage of the number of SF atomic layers as well as to the SF self-closure. High Angle Annular Dark Field-Scanning Transmission Electron Microscopy (HAADF-STEM) attested how the crystal tends to smooth out the lattice mismatch until the SF is suppressed. Because of the foregoing, the mechanisms of evolution of the defects in (111) 3C-SiC revealed in this study, demonstrates how the growth parameters must be matched with the kinetics of the defects in order to endorse (111) 3C-SiC adoption in high performing devices.

1. Introduction

3C-SiC is a particularly attractive SiC polytype since it has higher mobility and a lower density of states at the 3C-SiC/SiO_2 interface than 4H and 6H-SiC counterparts. These characteristics along with 2.5 eV bandgap make 3C-SiC suitable for power electronics applications, due to several benefits in MOS devices such as a notable R_{on} reduction for medium voltage applications working under 1200 V.

A large number of papers have been released on the development of SiC on Si using not only CVD but also sputtering or molecular beam epitaxy (MBE) [[1] [2] [3],], . Throughout the decades CVD was, however, preferred as it can produce high-quality 3C-SiC films with a larger area and thickness compared to MBE. CVD is, also, a more cost-effective method than MBE and can be used to grow 3C-SiC on a wider range of substrates, including silicon with a higher growth rate which can be useful for large-scale production.

Current technology is largely based on Si heteroepitaxial growth which thus involves 20% mismatch in the lattice parameter and 8% different thermal expansion coefficient [[4]]. As a consequence, several types of defects, such as dislocations, stacking faults (SFs) and grain boundaries nucleate close to the 3C-SiC/Si interface, both during the high temperature deposition and the cooling down driven by the misfit

* Corresponding author at: CNR-IMM, VIII Strada, 5,95121 Catania, Italy.
E-mail address: cristiano.calabretta01@st.com (C. Calabretta).

https://doi.org/10.1016/j.mee.2023.112116
Received 15 March 2023; Received in revised form 15 October 2023; Accepted 23 October 2023
Available online 25 October 2023

strain relaxation. In particular, 3C-SiC films grown on (111) Si substrates exhibit poor crystal quality and experience wafer cracks and bowing. Unlike growths along the [100] crystallographic direction the only difference between two conceivable stacking configurations along [111] is that the SiC tetrahedra are twisted 180° relative to the [111] direction, generating twins rather than anti-phase [[5,6,16]]. Severino et al. [[7]] reported a drastically lower SF density (about 1.7×10^4 cm^{-1} for a 7 mm-thick film) in 3C-SiC films grown on (111) off-axis Si substrates as a preliminary result, but the sample did barely release its strain via defect generation and displayed considerable wafer bowing. [[7,8]]. It is worthwhile to investigate other ways for producing thick (111) 3C-SiC films. Prior studies on the formation of (111) 3C-SiC adopted an epitaxial growth technique [[9], [10]] and selective epitaxy [[11]]. On the other hand, greater emphasis has been dedicated towards the research of compliant substrates. Porous Si [[12]], Silicon-on-Insulator [[13]], SiGe buffer layer [[14]], patterned substrates such as inverted Si pyramids (ISP) [[15]], and Si micropillars [[16]] represent few examples of compliant substrates which have been involved in 3C-SiC growth. Overall, both orientations have been studied extensively and revealed to be promising for various applications, however, the huge tensile stress, which builds up above first layer deposition, hinders the development of (111) 3C-SiC wafers with large surface area and considerable thickness as in (100) 3C-SiC, which has better defects and stress control [[17], [18]]. However the higher Young's modulus of [111] 3C-SiC makes it more suitable for applications that require high mechanical strength and stiffness, such as in microelectromechanical systems (MEMS) [[19]]. The growth of (111)-3C-SiC is also fundamental for the increase in the field of SiC heterojunctions as a two-dimensional electron gas (2DEG) can exist at the 3C-SiC/4H-SiC heterointerface [[20] [21] [22],],. It is also suitable as a substrate in GaN based devices for reducing the concentration of dislocations the quantity of cracks, avoiding meltback etching caused by the outdiffusion of $^{Si\ in\ GaN}$ [23,24,25].

On the basis of the achieved experience along the [001] orientation, the basic idea behind this research is to develop heteroepitaxially grown layer as a seed, through silicon substrate melting, and then proceed with high-temperature growth. As first attested in [[26]], the removal of the substrate eliminates the major source of stress caused by the lattice mismatch with Si and the difference in thermal expansion coefficient allowing a considerable rise in growth temperature, necessary for thicker wafers and higher quality material [[27]]. Moreover, N doping has previously shown to hinder the propagation of 4H and 6H-like SFs in 3C-SiC while also supplying compressive stress to the crystal [[28]' [29]].

As a result of these approaches, thicknesses up to 230 mm along the [111] direction are here documented. As far as we are concerned, this is the highest (111) oriented 3C-SiC epitaxial layer thickness on 4 in. wafer size ever achieved. Consequently, it was possible to evaluate the impact of varying growth temperatures on crystal quality in terms of point and extended defects, compare these findings with prior results obtained from the (100) oriented 3C-SiC growth direction, and unveil a distinctive mechanism for self-closure of stacking faults on (111) oriented 3C-SiC. The evolution dynamics of SFs along (111) 3C-SiC growths were attested as less effective in mutual annihilation of SFs, suggesting high growth temperatures as a reliable strategy to improve N activation and SFs self-closure.

2. Materials and methods

3C-SiC growth was performed in a horizontal hot-wall Chemical Vapor Deposition (CVD) reactor on a 4 in. Si substrate. Precursor gases were Tri-chloro-silane (TCS) and Ethylene (C_2H_4) with (H_2) as carrier gas. A two step growth process was applied with the carbonization plateau at 1160 °C followed by CVD growth step at 1400 °C. One (100) 4° off-axis wafer was grown with constant 314 sccm while another growth was performed on (111) oriented Si wafer and 1600 sccm N_2 flux. To increase crystal quality the process was first performed at a low growth rate of 3 μm/h for 30′, followed by another 30′ growth at 6 μm/h and then fast growth rate of 30 μm/h was carried out until a ~ 75 μm layer was reached. Afterwards, Si substrate was melted at 1600 °C in the reactor. The remaining freestanding SiC wafer was used as a seed layer for subsequent homoepitaxial growth at 1600 °C. A growth rate of 60 μm/h for two hours was used to increase the substrate thickness. Final 30 μm were grown intrinsic (Not Intentional Doped) in order to design a device geometry. Molten KOH etching at 500 °C for 3′ was performed on uniformly lapped sample in order to provide a comprehensive examination of crystal defects through SEM microscopy in-plane analysis at 75 μm and at 230 μm following hetero and homoepitaxial bulk growth respectively. Micro-Photoluminescence (μ-PL) was performed through Horiba Jobin Yvon HR800 spectrometer (Horiba, Lille, France) integrated system under backscattering configuration. The excitation wavelength was supplied by a 325 nm He—Cd continuous-wave laser that was focalized on the sample by a 40× objective, with a numerical aperture (NA) of 0.5. The scattered light was dispersed by a 300 grooves/mm kinematic grating. To carry out a scan at different penetration depths in the grown surface layer Horiba Fluorolog spectrofluorimeter equipped with a 400 W Xe lamp was used. The excitation wavelength was varied between 300 nm and 500 nm. To explore SFs evolution in (111) 3C-SiC growth, TEM investigations were carried out on a JEOL JEM 2010F TEM-FEG operating at 200 kV microscope. High Angle Annular Dark Field Scanning Transmission Electron Microscopy (HAADF-STEM) images were acquired through ARM200F probe Cs-corrected TEM, equipped with a cold field emission gun (FEG) and working at 200 kV with a nominal resolution of 0.68 Å. HAADF-STEM micrographs were obtained with intensities nearly proportional to the atomic number Z^2 allowing for a sensible mass contrast.

3. Results and discussion

Wet etching reveals the existence of SFs due to the variation of the etching rate, which stimulates groove generation along the extension of the extra planes relying on the change of binding energy in the presence of defects [[30]] and, in this regard, is crucial to identify SFs on the studied surfaces.

SFs density variation is visually attested in Fig. 1 which exhibits two SEM images of (100) and (111) oriented 3C-SiC surfaces acquired post molten KOH etching after homoepitaxial growth. In Fig. 1a the detection of parallel SFs in a single direction is motivated by two reasons: (i) the preferential SFs nucleation direction induced by the off-axis (100) growth direction and (ii) by the preferential etching following binding energy difference within Si-terminated SF (SF_{Si}) and C-terminated ones (SF_C). For statistical analyses, we will consider this family of SFs (like those indicated by arrows in Fig. 1(a)). Coherently with the growth direction, Fig. 1b, on the other hand, shows SFs in (111) 3C-SiC appearing as lines that compose sides of equilateral triangles, and therefore the impact of preferred etching defines 60° angles relative to each other. For geometric considerations, the SFs share the same polarity and so belong to the same C-face family as (111) 3C-SiC is Si face.

The SEM inspections on the samples subjected to KOH attack enabled the density of SFs within the grown samples to be assessed. The results are reported in Fig. 2. The length distributions of the SFs were fitted with log-normal type curves, which are better suited to fitting the experimental results and reducing error as stated in [28]. The mean lengths of the SFs were determined using the fits for all the samples. The average length of the SFs in off-axis (100) 3C-SiC was 0.31 ± 0.01 mm, with a density of $(2.47 \pm 0.09) \times 10^3$ cm^{-1}.

The growth of (111) 3C-SiC exhibits a different trend. On the one hand, the heteroepitaxial growth shows a surface density of SFs as high as $(7.16 \pm 0.04) \times 10^3$ cm^{-1}. Despite the increased flow of N compared to the (100) 3C-SiC growth, the sample clearly exhibits a higher SFs density. The average length of the SFs can be estimated from the fit of the distribution as 3.32 ± 0.35 mm. At 230 mm growth, the density of

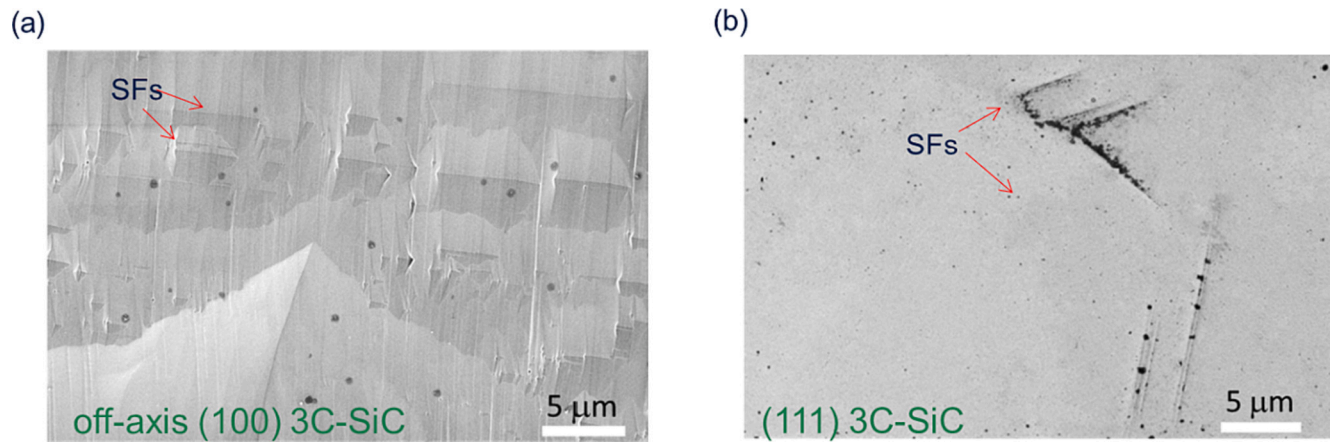

Fig. 1. SEM images after molten KOH etching highlighting SFs of (a) off-axis (100) 3C-SiC growth and (b) (111) 3C-SiC growth.

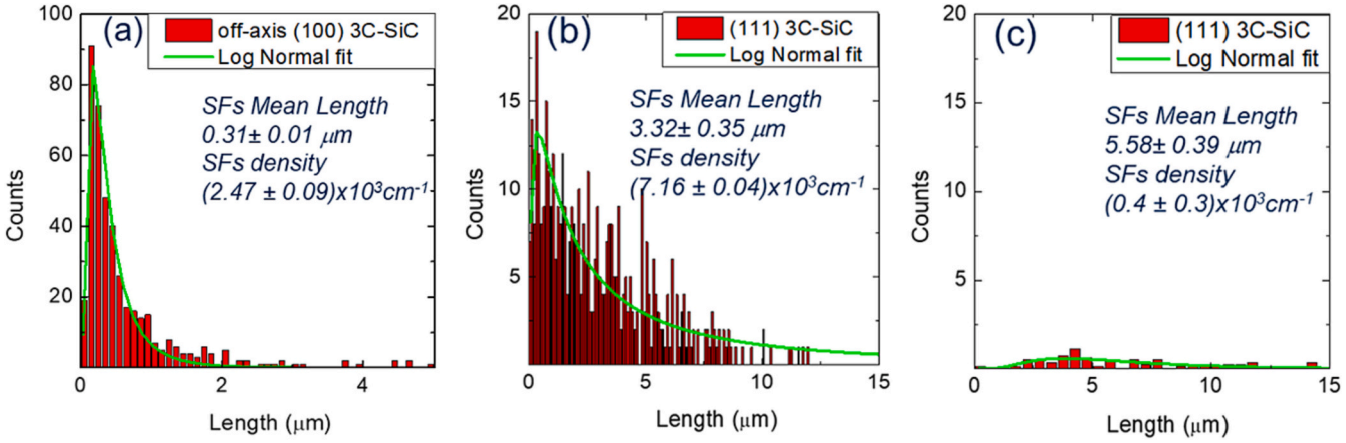

Fig. 2. SFs histogram for off-axis (100) 3C-SiC (a) after homoepitaxial growth, for (111) 3C-SiC (b) after heteroepitaxial growth and (c) after homoepitaxial growth.

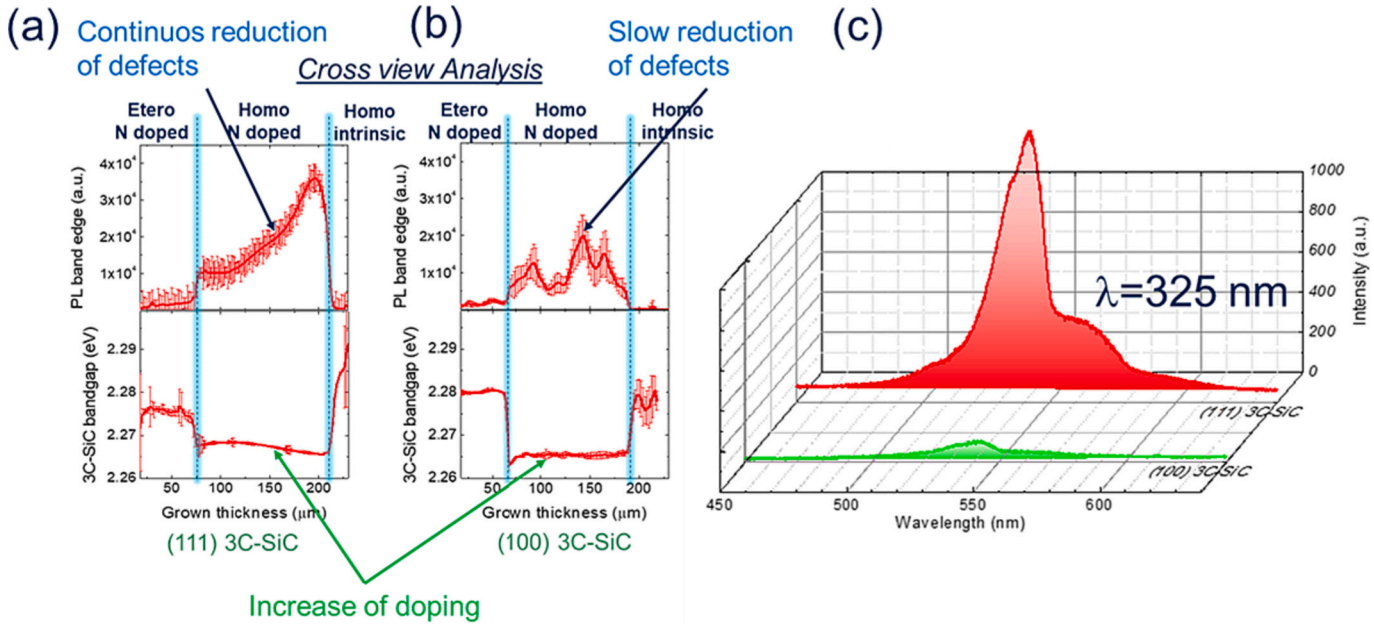

Fig. 3. Intensity (upper panel) and emission wavelength (lower panel) of the PL peak as a function of grown thickness for the two homoepitaxies of (a) (100) 3C-SiC and (b) (111) 3C-SiC acquired in cross configuration. (c) In plane photoluminescence spectrum showing the band to band region for the (100) 3C-SiC sample and for the (111) 3C-SiC sample.

SFs drops to (0.4 ± 0.3) × 10^3 cm^{-1}. As a result, it appears that the homoepitaxial growth phase is crucial for crystal improvement. The mean length of the SFs grows to 5.58 ± 0.39 mm, which is consistent with the reduction of intersection and mutual exclusion events in the propagation of SFs.

This behavior is supported by acquisitions in Fig. 3a which reports in the upper panel the average intensity of the band edge peak extracted from the μ-PL map in cross configuration for both samples. In the case of (111) 3C-SiC growth, starting from 75 μm there is a consistent increase in the band-to-band recombination signal following the increase of the N doping activation in the crystal during the 1600 °C growth step. This process is accompanied by the shrinkage of the bandgap displayed in the panel below of Fig. 3a where the graph depicts the relative emission wavelength of the band-to-band peak as a function of grown thickness aligned with the band to band peak intensity plot. As the growth progresses, a steep enhancement of the band-to-band peak is observed with a higher slope than the heteroepitaxial growth phases. Following the fairly constant bandgap amplitude in the two respective growth segments, it is possible to prevalently attribute the strong increase in band-to-band recombination to the improvement of the crystal quality and to the consequent reduction of SFs density and of other recombination center during the growth at 1600 °C. The same method was adopted for the (100) 3C-SiC sample (Fig. 3b). The emission intensity is modest, similarly to the prior one. When the region exposed to homoepitaxial growth is involved in the inspection, the intensity of the PL rises, corresponding to a drop in the emission wavelength of the bandgap. The drop of band-to-band emission to lower wavelength also shows that raising the growth temperature to 1600 °C increased the incorporated dopant fraction. However, in contrast to growth (111), a slower and fluctuating defect recovery pattern is observed from band-to-band peak, outlining a mechanism of evolution of the crystal not characterized by the steep improvement highlighted by the trend for the growth of (111) 3C-SiC in Fig. 3a. Fig. 3c depicts the in plane PL spectra acquired on the surface of the two samples under laser excitation λ = 325 nm. It is worth noting that in this circumstance, the area under investigation correspond exclusively to the intrinsically grown regions. The band-to-band 3C-SiC peak obtained in the (111) growth direction grown sample is a factor of ten greater than the corresponding (3C-SiC) peak obtained in the (100), revealing a considerable increase in crystal quality.

A further spectral region investigated is reported in Fig. 4. Here the superimposition of the spectral emissions in the near IR of the samples acquired at different wavelengths is reported. These regions are related to the emission of point defects in 3C-SiC and the scanning along different wavelengths allowed to acquire the spectra at different depths (from 2 to 33 μm) so as to acquire the signal coming from the intrinsic region of the homoepitaxies and compare the emissions of the two samples in this spectral region. Fig. 4a shows this overlap with respect to the (100) 3C-SiC sample. It can be seen that the sample has a prominent defect band along the entire scanned section. The emission band is slightly reduced in intensity in contact with the doped region under the 30 μm intrinsic region. On the other hand, it can be noted that the 3C-SiC growth on [111] direction does not present this band of defects along the entire investigated thickness. This absence of the emission band can be correlated with the large difference between the PL signals in the previously observed band-to-band emission region. The absence of recombination centers given by the point defects justifies the strong emission of the (111) compared to the (100) oriented sample. The most accredited interpretation for the origin of this peak at 0.884 eV leads back to the ionization level of the nitrogen-vacancy (NV) center in 3C-SiC, in which the substitutional N_C sits next to a Si vacancy $(N_C–V_{Si})^-$ defects [[31] [32] [33],] ,.

STEM analyses in the cross section were performed to better understand the evolution of the defects within the (111) 3C-SiC sample, and in particular to describe the evolution of the density of the SFs during growth after the homoepitaxy process as assessed in Fig. 2b. The control over defectiveness of (111) 3C-SiC growth is shown by the different evolution modalities of the SFs in the (111) oriented crystal. In the [110] zone axis acquisition, a SF lying along the plane (−11−1) is observed in section as a white line, along with two SFs lying on the planes (−1−11). Fig. 5a displays a STEM image of the (111) 3C-SiC sample obtained in the central section of the homoepitaxially grown area. It appears evident how the typical mechanism valid in (100) growths consisting in the mutual closure of SFs coming from opposing {111} planes that give rise to Lomer and λ-shaped dislocations [[34]] is replaced by a different panorama of evolution.

Indeed, Fig. 5a shows how SFs shred but do not interrupt each other instead barely interfere during growth, allowing them to continue expanding despite the intersection. Additionally, red arrows show white contrasted zones. These regions could be present within the SFs, either to mark the end of the defect itself, as indicated by the arrow on the lower left in Fig. 5a, or they can be linked to the intersection of a new SF, as indicated by the yellow arrow on the top right. The above reported white contrasted region was noticed to be highly common in the homoepitaxial region, but it was also confirmed to be present in the superficial intrinsic region, as shown in Fig. 5b, where one of the two SFs lying along the (−11–1) plane is affected by a light contrast perturbation and continues to propagate towards the surface. Through HAADF-STEM investigation it was therefore possible to attest the atomic structure of SFs in the vicinity of this type of defect. It must be preliminarly stated that SFs observed in 3C-SiC can be classified into three classes based on the amount of atomic planes containing the incorrect configuration of the Si—C dimers with respect to the perfect crystal [[35,36]]. <SF1>, <SF2>, and < SF3>, respectively, are built up of one, two, or three faulted atomic planes and are known as intrinsic, extrinsic, and

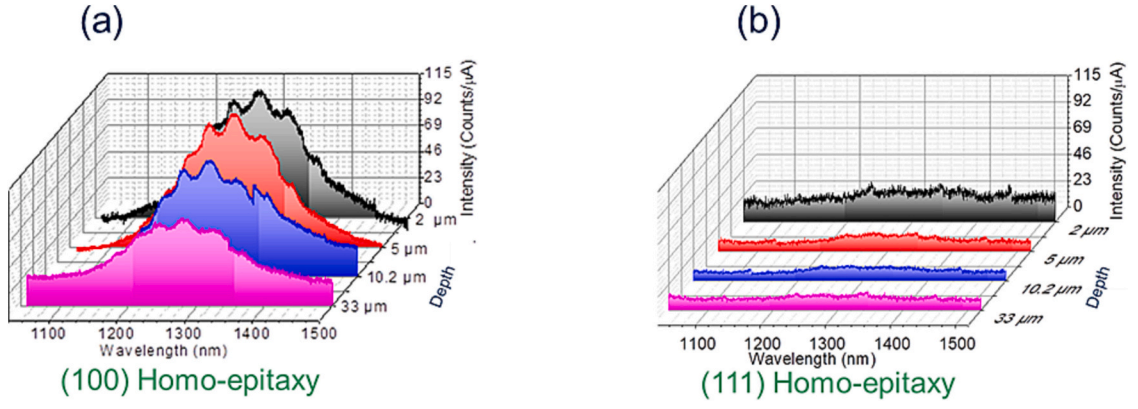

Fig. 4. Photoluminescence in spectral range correlated to point defects at different thicknesses of the intrinsic grown region for (a) (100) 3C-SiC and (b) (111) 3C-SiC sample.

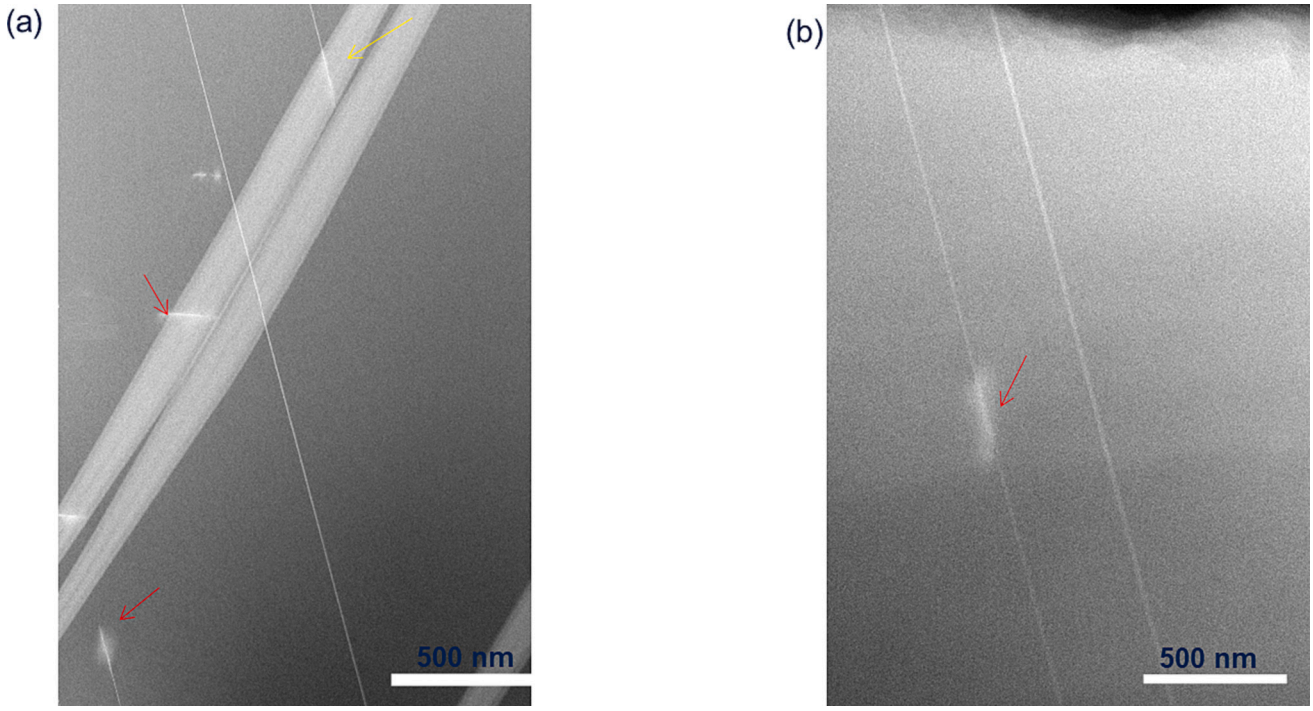

Fig. 5. Bright Field TEM of (111) 3C-SiC (a) in the homoepitaxial region grown with 1600 sccm N_2 flux and (b) in the near-surface intrinsic zone.

conservative SFs. Fig. 6a shows a double SF characterized by a shift of 2/3[001] along the c axis. It can be seen how a mismatch is created between the planes of the regular crystal present on the right and on the left, represented by the plane marked in yellow. This plane involves the reduction of a layer of the SF implying the passage from <SF2> to <SF1>. This plane, therefore, constitutes the partial dislocation that surrounds the atomic plane which has stopped propagating. Following the sample in Fig. 6b, the occurrence of the same phenomenon is recorded, in which an extra-plane present inside the crystalline lattice represents a further partial dislocation surrounding the SF and determining the interruption of its propagation.

The crystal thus continues to grow without the SF. This type of closure appears very frequent within the homoepitaxial region and seems to be a phenomenon strongly influencing the growth of 3C-SiC in that region. It is, therefore, possible to assert that this phenomenon appears to be a key factor in the improvement of the crystalline quality and according to the statistics conducted on the sample, appears to be characteristic of (111) 3C-SiC growths and hence substitute for the reciprocal annihilation of the SFs across opposing planes observed within the (100) grown 3C-SiC. Density-functional theory (DFT) simulations [29] suggested the increase of SF formation energy by rising doping level in 3C-SiC. Unfortunately, the precise placement of the nitrogen atoms is unknown. According to models, the dopant's impact is quite narrow, spanning around 10 Å. Additionally, because 3C has the shortest Si—C bond length along the [111] growth direction, significant inclusion of N on the (111) oriented surface stabilizes the cubic polytype along this favored direction, as observed by Lorenzzi et al. [[37]]. Variations in SiC stoichiometry are caused by high N activation. According to a macroscopic standpoint, the substitutional integration of N on C sites promotes a rise of the N_{Si}/N_C ratio (where N_{Si}/N_C are the number of silicon atoms and carbon atoms) which stabilizes 3C-SiC [[38]]. This phenomenon appears, in the case of (111) 3C-SiC growths, stimulated by the increase in temperature and by the consequent increase in incorporation of N into 3C-SiC, since only substitutional N appears to play an active role in the closure of SFs [[39]].

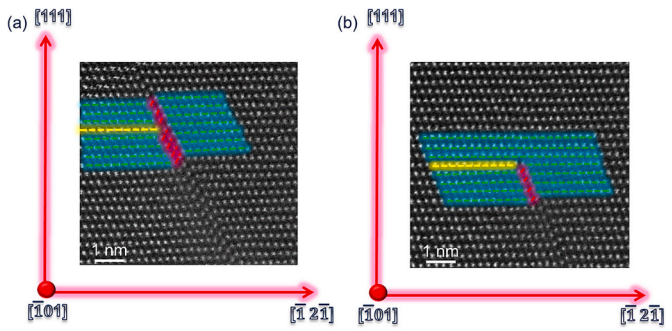

Fig. 6. HAADF-STEM displaying the evolution of a SF from (a) two layer SF to a single layer SF and (b) from a single layer SF to its closure.

The crystal tends to smooth out the lattice mismatch until the SF is suppressed. Because of the foregoing, the mechanisms of evolution of the defects in (111) 3C-SiC revealed in this study, demonstrates how the growth parameters must be matched with the kinetics of the defects in order to endorse (111) 3C-SiC adoption in high performing devices.

4. Conclusions

In this work a pioneering bulk growth of (111) 3C-SiC is reported. By growing on a 4 in. Si substrate a 75 μm thick seed was obtained. Once the Si was melted, the bulk homoepitaxial growth took place which allowed to grow 230 μm thick (111) 3C-SiC layer under 1600 sccm N_2 flow. From molten KOH etching it was attested a conspicuous drop in the density of SFs between the heteroepitaxial and homoepitaxial phases, thanks to the increase in the fraction of N incorporated in the crystal. The m-PL investigations exhibited a sharp rise in the intensity of the band-edge signal of the crystal and an increase of a factor of 10 in the intensity of surface emission compared to a sample of the same thickness grown along the (100) direction. Noteworthy is the difference in terms of near-infrared emission which attests the low concentration of point defects of (111) 3C-SiC sample compared to the (100) 3C-SiC. The HAADF-STEM analyses allowed to disclose the existence of a self-closure mechanism of the SFs showing how the crystal tends to smooth out the lattice mismatch until the SF is suppressed.

CRediT authorship contribution statement

C. Calabretta: Conceptualization, Methodology, Formal analysis, Investigation, Data curation, Writing – original draft. **V. Scuderi:** Methodology, Investigation, Writing – review & editing. **C. Bongiorno:** Methodology, Data curation, Investigation. **R. Anzalone:** Visualization. **R. Reitano:** Data curation. **A. Cannizzaro:** Data curation. **M. Mauceri:** Visualization. **D. Crippa:** Project administration. **S. Boninelli:** Formal analysis, Data curation, Writing – review & editing. **F. La Via:** Conceptualization, Investigation, Supervision, Project administration, Funding acquisition.

Declaration of Competing Interest

The authors declare that they have no known competing financial interests or personal relationships that could have appeared to influence the work reported in this paper.

Data availability

Data will be made available on request.

Acknowledgements

This project has received funding from the European Union's Horizon 2020 research and innovation program under grant agresteeeement No 823717 – ESTEEM3.

This work has been partially funded by European Union (NextGeneration EU), through the MUR-PNRR project SAMOTHRACE (ECS00000022).

This research was partially funded by the European Union within the framework of the project CHALLENGE, grant number 720827, and SiC nano for PicoGeo, grant agreement number 863220.

References

[1] Jörg Pezoldt, et al., Carbonization induced change of polarity for MBE grown 3C-SiC/Si (111), Mater. Sci. Forum 353 (2001).
[2] A. Fissel, et al., MBE-growth of heteropolytypic low-dimensional structures of SiC, Thin Solid Films 380 (1–2) (2000) 89–91.
[3] Shigeo Kaneda, et al., The growth of single crystal of 3C-SiC on the Si substrate by the MBE method using multi electron beam heating, Jpn. J. Appl. Phys. 25 (9R) (1986) 1307.
[4] F. La Via, A. Severino, R. Anzalone, C. Bongiorno, G. Litrico, M. Mauceri, M. Schoeler, P. Schuh, P. Wellmann, From thin film to bulk 3C-SiC growth: understanding the mechanism of defects reduction, Mater. Sci. Semicond. Process. 78 (2018) 57–68.
[5] A. Severino, et al., Preferential oxidation of stacking faults in epitaxial off-axis (111) 3C-SiC films, Appl. Phys. Lett. 95 (2009) 11.
[6] Zhe Chuan Feng, et al., Structural characteristics of 3C–SiC thin films grown on Si-face and C-face 4H–SiC substrates by high temperature chemical vapor deposition, Vacuum 207 (2023), 111643.
[7] A. Severino, M. Camarda, G. Condorelli, L.M.S. Perdicaro, R. Anzalone, M. Mauceri, A. La Magna, F. La Via, Effect of the miscut direction in (111) 3 C-Si C film growth on off-axis (111) Si, Appl. Phys. Lett. 94 (10) (2009), 101907.
[8] A. Severino, C. Bongiorno, N. Piluso, M. Italia, M. Camarda, M. Mauceri, G. Condorelli, et al., High-quality 6 inch (111) 3C-SiC films grown on off-axis (111) Si substrates, Thin Solid Films 518 (6) (2010) S165–S169.
[9] Yoichi Okui, Chacko Jacob, Satoru Ohshima, Shigehiro Nishino, Control of pendeo epitaxial growth of 3C-SiC on silicon substrate, in: Materials Science Forum vol. 433, Trans Tech Publications Ltd, 2003, pp. 209–212.
[10] A. Shoji, Yoichi Okui, Taro Nishiguchi, Satoru Ohshima, Shigehiro Nishino, Pendeo epitaxial growth of 3C-SiC on Si substrates, in: Materials Science Forum vol. 457, Trans Tech Publications Ltd, 2004, pp. 257–260.
[11] Yoichi Okui, Chacko Jacob, Satoru Ohshima, Shigehiro Nishino, Selective epitaxial growth of pyramidal 3C-SiC on patterned Si substrate, in: Materials Science Forum vol. 389, Trans Tech Publications Ltd., Zurich-Uetikon, Switzerland, 2002, pp. 331–334.
[12] Philip G. Neudeck, J. Anthony Powell, Andrew J. Trunek, David J. Spry, Step free surface heteroepitaxy of 3C-SiC layers on patterned 4H/6H-SiC mesas and cantilevers, in: Materials Science Forum vol. 457, Trans Tech Publications Ltd, 2004, pp. 169–174.
[13] Jessica Eid, Irina G. Galben-Sandulache, Georgios Zoulis, Teddy Robert, Didier Chaussende, Sandrine Juillaguet, Antoine Tiberj, Jean Camassel, Nitrogen doping of 3C-SiC single crystals grown by CF-PVT, in: Materials Science Forum vol. 615, Trans Tech Publications Ltd, 2009, pp. 45–48, 7.
[14] M. Zimbone, M. Zielinski, E.G. Barbagiovanni, C. Calabretta, F. La Via, 3C-SiC grown on Si by using a Si1-xGex buffer layer, J. Cryst. Growth 519 (2019) 1-6.6.
[15] Massimo Zimbone, Marcin Zielinski, Corrado Bongiorno, Cristiano Calabretta, Ruggero Anzalone, Silvia Scalese, Giuseppe Fisicaro, Antonino La Magna, Fulvio Mancarella, Francesco La Via, 3C-SiC growth on inverted silicon pyramids patterned substrate, Materials 12 (20) (2019) 3407.
[16] M. Agati, S. Boninelli, C. Calabretta, F. Mancarella, M. Mauceri, D. Crippa, M. Albani, R. Bergamaschini, L. Miglio, F. La Via, Growth of thick [111]-oriented 3C-SiC films on T-shaped Si micropillars, Mater. Des. 208 (2021), 109833.
[17] Zhe Cheng, et al., High thermal conductivity in wafer-scale cubic silicon carbide crystals, Nat. Commun. 13 (1) (2022) 7201.
[18] Via Francesco La, et al., New approaches and understandings in the growth of cubic silicon carbide, Materials 14 (18) (2021) 5348.
[19] Sergio Sapienza, et al., Measurement of residual stress and Young's modulus on micromachined monocrystalline 3C-SiC layers grown on ⟨111⟩ and ⟨100⟩ silicon, Micromachines 12 (9) (2021) 1072.
[20] Yuchen Shi, et al., A comparative study of high-quality C-face and Si-face 3C-SiC (111) grown on off-oriented 4H-SiC substrates, J. Phys. D. Appl. Phys. 52 (34) (2019), 345103.
[21] Hiroyuki Sazawa, Hirotaka Yamaguchi, High-mobility 2D electron gas in carbon-face 3C-SiC/4H-SiC heterostructure with single-domain 3C-SiC layer, Appl. Phys. Lett. 120 (2022) 21.
[22] Valdas Jokubavicius, et al., Lateral enlargement growth mechanism of 3C-SiC on off-oriented 4H-SiC substrates, Cryst. Growth Des. 14 (12) (2014) 6514–6520.
[23] Mario F. Zscherp, et al., AlN buffer enhances the layer quality of MBE-grown cubic GaN on 3C-SiC, Cryst. Growth Des. 22 (11) (2022) 6786–6791.
[24] Stefano Leone, et al., Epitaxial growth optimization of AlGaN/GaN high electron mobility transistor structures on 3C-SiC/Si, J. Appl. Phys. 125 (2019) 23.
[25] Masayoshi Katagiri, et al., MOVPE growth of GaN on Si substrate with 3C-SiC buffer layer, Jpn. J. Appl. Phys. 53.5S1 (2014) 05FL09.
[26] Ruggero Anzalone, Massimo Zimbone, Cristiano Calabretta, Marco Mauceri, Alessandra Alberti, Riccardo Reitano, Francesco La Via, Temperature investigation on 3C-SiC homo-epitaxy on four-inch wafers, Materials 12 (20) (2019) 3293.
[27] Via Francesco La, et al., New approaches and understandings in the growth of cubic silicon carbide, Materials 14 (18) (2021) 5348.
[28] Cristiano Calabretta, Viviana Scuderi, Ruggero Anzalone, Marco Mauceri, Danilo Crippa, Annalisa Cannizzaro, Simona Boninelli, Francesco La Via, Effect of nitrogen and aluminum doping on 3C-SiC Heteroepitaxial layers grown on 4 off-Axis Si (100), Materials 14 (16) (2021) 4400.
[29] Yoshitaka Umeno, Kuniaki Yagi, Hiroyuki Nagasawa, Ab initio density functional theory calculation of stacking fault energy and stress in 3C-SiC, Phys. Status Solidi B 249 (6) (2012) 1229–1234.
[30] N.G. Van der Berg, Johan B. Malherbe, A.J. Botha, E. Friedland, Thermal etching of SiC, Appl. Surf. Sci. 258 (15) (2012) 5561–5566.
[31] Anderson Janotti, L. Gordon, Chris G. Van de Walle, Defects as Qubits in 3C-and 4H-SiC, 2015.
[32] A. Csóré, H.J. von Bardeleben, J.L. Cantin, A. Gali, Characterization and Formation of NV Centers in 3C, 4H and 6H SiC: an\emph {ab initio} Study, arXiv preprint arXiv:1705.06229, 2017.
[33] Michael Schöler, Maximilian W. Lederer, Philipp Schuh, Peter J. Wellmann, Intentional incorporation and tailoring of point defects during sublimation growth of cubic silicon carbide by variation of process parameters, Phys. Status Solidi B 257 (1) (2020) 1900286.
[34] J. Yamasaki, S. Inamoto, Y. Nomura, H. Tamaki, N. Tanaka, Atomic structure analysis of stacking faults and misfit dislocations at 3C-SiC/Si (001) interfaces by aberration-corrected transmission electron microscopy, J. Phys. D. Appl. Phys. 45 (49) (2012), 494002.
[35] Massimo Zimbone, Andrey Sarikov, Corrado Bongiorno, Anna Marzegalli, Viviana Scuderi, Cristiano Calabretta, Leo Miglio, Francesco La Via, Extended defects in 3C-SiC: stacking faults, threading partial dislocations, and inverted domain boundaries, Acta Mater. 213 (2021), 116915.
[36] Luca Barbisan, Andrey Sarikov, Anna Marzegalli, Francesco Montalenti, Leo Miglio, Nature and shape of stacking faults in 3C-SiC by molecular dynamics simulations, Phys. Status Solidi B 258 (6) (2021) 2000598.
[37] Jean Lorenzzi, Veronique Souliere, Davy Carole, Nikoletta Jegenyes, Olivier Kim-Hak, François Cauwet, Gabriel Ferro, Effect of nitrogen impurity on the stabilization of 3C–SiC polytype during heteroepitaxial growth by vapor–liquid–solid mechanism on 6H–SiC substrates, Diam. Relat. Mater. 20 (5–6) (2011) 808–813.
[38] Yu M. Tairov, V.F. Tsvetkov, Growth of bulk silicon carbide single crystals, Growth Cryst. (1993) 37–46.
[39] Cristiano Calabretta, Viviana Scuderi, Corrado Bongiorno, Annalisa Cannizzaro, Ruggero Anzalone, Lucia Calcagno, Marco Mauceri, Danilo Crippa, Simona Boninelli, Francesco La Via, Impact of nitrogen on the selective closure of stacking faults in 3C-SiC, Cryst. Growth Des. 22 (8) (2022) 4996–5003.